Reaction Kinetics, Mechanisms and Catalysis (2019) 127:187–203
https://doi.org/10.1007/s11144-019-01572-2

Water–gas shift reaction over gold deposited on NiAl layered double hydroxides

Margarita Gabrovska[1] · Tatyana Tabakova[1] · Ivan Ivanov[1] · Daniela Kovacheva[2]

Received: 7 January 2019 / Accepted: 29 March 2019 / Published online: 5 April 2019

Abstract

Three samples of NiAl layered double hydroxides with takovite-like structure were prepared by a co-precipitation method at Ni^{2+}/Al^{3+} molar ratios of 1.5, 2.5 and 4.0. The samples were investigated as catalysts for hydrogen production by means of water–gas shift reaction (WGSR). The properties and catalytic behavior of the unmodified as-synthesized materials are compared with those of the same materials used as a support on which gold particles have been deposited. All samples were characterized by N_2 physisorption, Powder X-ray diffraction (PXRD), and X-ray photoelectron spectroscopy (XPS) techniques. Catalytic activity of all materials was studied towards conversion of CO at atmospheric pressure within the temperature interval 140–300 °C. The dependence of WGS activity on the Ni^{2+}/Al^{3+} molar ratio and the presence of gold were investigated. The promotional role of Au on the WGS performance was clearly demonstrated by Au–NiAl2.5 catalyst, which reached equilibrium conversion value of 97.6% at 240 °C. The stability test of the most active Au–NiAl2.5 catalyst resulted in the same CO conversion degree within 32 h under stream at 260 °C. A plausible scheme for the reaction mechanism, including the redox $Ni^{2+} \leftrightarrow Ni^{3+}$ transition on the catalyst surface as well as adsorption and activation of the CO molecule on the Au particles, is proposed.

Keywords NiAl layered double hydroxides · Gold catalysts · NiAl mixed metal oxides · CO conversion by water–gas shift reaction

✉ Margarita Gabrovska
margarita.gabrovska@abv.bg; margo@ic.bas.bg

[1] Institute of Catalysis, Bulgarian Academy of Sciences, Acad. G. Bonchev Str., Bldg. 11, 1113 Sofia, Bulgaria

[2] Institute of General and Inorganic Chemistry, Bulgarian Academy of Sciences, Acad. G. Bonchev Str., Bldg. 11, 1113 Sofia, Bulgaria

Introduction

The conversion of CO by water vapor, named water–gas shift reaction ($CO + H_2O \leftrightarrow CO_2 + H_2$) is one of the economic routes traditionally applied for the reduction of CO in the synthesis gas and production of pure hydrogen. Hydrogen purification is a key point aiming to prevent the CO catalyst poisoning effect especially in the fuel cell anode technology as well as in the selective hydrogenation processes [1, 2].

Industrially, WGSR is carried out in two stages with two different oxide catalysts with interstage cooling. The first stage of WGSR takes place in the interval 350–450 °C over Fe_2O_3–Cr_2O_3 oxide catalyst resulting in CO residual of about 2–5% and is named high-temperature (HT) shift. The second one is so-called low-temperature (LT) shift because operates between 180 and 250 °C decreasing the CO concentration below 1% over Cu–ZnO–Al_2O_3 catalyst. The equilibrium CO conversion diminishes with the increase of reaction temperature due to the exothermic character of the reaction ($\Delta H_{300^\circ C} = -41.2$ kJ/mol). Consequently, high temperature is not advantageous for attaining high degree of CO conversion and hydrogen production [3]. However, Cu-containing catalysts are very sensitive to thermal sintering. In this regard, attempts have been made of researchers to develop modified Fe- and Cu-based catalysts with improved catalytic behavior as well as more effective, thermally stable, non-pyrophoric and low-priced new ones for both temperature stages [4]. On the other hand, an important task for research community is to create catalysts active enough to carry out the process at intermediate temperatures.

Considering both the price and the necessity to advance new catalyst compositions that operate at intermediate temperatures, particular attention was focused on Ni-based catalysts. In our previous work [5], the development of nickel hydroxide supported on activated charcoal as WGS catalyst was reported for the first time. The catalyst exhibited higher activity in comparison with Cu-containing catalyst under the same reaction conditions. Further, it was established that co-precipitated NiAl layered double hydroxides (LDH), alone or promoted either by magnesium [6] or potassium [7] were active catalysts for medium-temperature WGSR.

Nevertheless, the variety of the catalytic systems described as active in the WGS reaction, Au-containing catalysts appeared to be the most promising systems to substitute the traditional catalysts for small-scale applications. In recent years, gold-based catalysts have received extended attention since they show very high activity at low temperatures and potential stability in oxidizing atmospheres [8, 9]. As it has been published, supported Au on different oxide carriers as Fe_2O_3, ZrO_2, TiO_2, CeO_2, doped-CeO_2, etc. displayed very high WGS activity at low temperatures [10–16].

NiAl LDHs, also referred to as takovite-like (TKl) compounds, according to the name of mineral takovite, $Ni_6Al_2(OH)_{16}CO_3{\cdot}4H_2O$ [17] are lamellar nanostructured materials which belong to a large group of natural or synthetic inorganic layered compounds. The structure consists of consequent positively charged brucite-like NiAl hydroxide sheets $\left[Ni^{2+}_{1-x}Al^{3+}_{x}(OH)_2\right]^{x+}$ and interlayers $\left[A^{n-}_{x/n}mH_2O\right]$, containing charge compensating exchangeable anions ($A = NO_3^-$, SO_4^{2-}, CO_3^{2-}, Cl^-, etc.) and m molecules of water. Here, x represents the fraction

of the Al^{3+} ion. The role of co-intercalated water molecules is to prevent the repulsion of interlayer anions. The lamellar structure supposes uniform distribution of the octahedrally coordinated Ni^{2+} and Al^{3+} cations in the hydroxide layer [17, 18]. Despite the statement that formation of single-phase stable LDH structure is realized only for a narrow range of Ni^{2+}/M^{3+} molar ratio between 2 and 3 [18], it was reported existence of LDH structure in wider interval, Ni^{2+}/M^{3+} molar ratio = 1.5–4 [19].

It should be noted that upon controlled thermal treatment of NiAl LDHs, the layered structure destroys with formation of NiAl mixed metal oxides. The decomposition products are characterized with high surface area, good distribution of both ions, nanometrical crystal size, high metal dispersion after reduction and stability against sintering [18]. The well-known property of Ni and Al ions to stay associated with one another through the calcination and reduction of the TKl compounds is a reason for their systematic study as catalyst precursors and nowadays [18, 20–22].

The aim of this paper is to present new data related to the investigation of the NiAl LDHs with different Ni^{2+}/Al^{3+} molar ratios as catalyst precursors for WGSR. An extension of our piece of research is to apply NiAl LDHs as supports of gold catalysts in order to improve the NiAl activity thus to obtain promising catalyst for WGSR. On the base of the mentioned considerations, the role of Ni loading (Ni^{2+}/Al^{3+} molar ratio) and the presence of gold on the WGS performance was examined.

Experimental

Sample preparation

Co-precipitation of NiAl samples

All the reagents are of '*pro analyze*' purity grade and procured by Alfa Aesar, USA.

NiAl TKl samples were synthesized with Ni^{2+}/Al^{3+} molar ratio of 1.5, 2.5 and 4.0 by co-precipitation employing $Ni(NO_3)_2{\cdot}6H_2O$, $Al(NO_3)_3{\cdot}9H_2O$, and Na_2CO_3 as precipitant.

An appropriate volume of distilled water was placed in a five-necked glass reactor equipped with a steam jacket, stirrer, pH electrode, thermocouple and reflux condenser, heated to 80 °C and adjusted with 0.9 M Na_2CO_3 solution to reach pH 8.0. The mixed NiAl solution (total metal concentration 0.5 M) and the precipitant were introduced drop-wise simultaneously to the reactor controlled by two peristaltic pumps (solutions feed flow rate of 1 L/h) under stirring at 300 rpm. The resulting slurry was aged for 60 min in the mother liquor under the above mentioned stirring rate, pH and temperature. It was then filtered off, thoroughly washed with hot distilled water until the pH of the filtrate decreased to ≈ 6–7 and absence of NO_3^- ions (testing with solution of diphenylamine in H_2SO_4). The precipitate was then dried at 80 °C for 20 h and named as-synthesized samples, designated as NiAlz, where *z* represents the Ni^{2+}/Al^{3+} molar ratio, for example NiAl2.5 (Table 1).

Table 1 The sample notation and the chemical composition of the as-synthesized samples

Sample	Ni^{2+}/Al^{3+} molar ratio	Chemical composition (wt%)		
		NiO	Al_2O_3	Au
NiAl1.5	1.48	68.4	31.6	–
NiAl2.5	2.49	78.5	21.5	–
NiAl4.0	4.02	85.5	14.5	–
Au–NiAl2.5	2.50	76.7	20.9	2.4
Au–NiAl4.0	4.00	83.3	14.2	2.5

Deposition of gold

Gold-containing samples were prepared by deposition–precipitation of gold on the selected NiAl LDH samples. NiAl material was suspended in distilled water by means of ultrasound, thereafter, the deposition of Au was performed by simultaneous addition of two aqueous solutions, precisely 0.06 M $HAuCl_4 \cdot 3H_2O$ as a gold precursor and 0.2 M Na_2CO_3 as a precipitation agent. The interaction was accomplished at 60 °C and pH 7.0 under stirring at 250 rpm and reactant feed flow rate of 0.15 L/h. The amount of gold (3 wt%) was chosen on the basis of previous investigation about the effect of gold content on the WGS activity [23]. After aging at 60 °C for 60 min, the material was filtered and carefully washed until removal of Cl^- ions. Au-containing solids were dried under vacuum at 80 °C and designated as *y*-NiAl*z*, where *y* denotes Au, for example Au–NiAl2.5.

Sample characterization

The chemical composition of the as-synthesized NiAl materials was determined by inductively coupled plasma atomic emission spectroscopy (ICP-AES) by JY (Jobin–Yvon) 38 spectrometer.

The phase composition of the as-synthesized and post WGSR samples (spent catalysts) were established by powder X-ray diffraction (PXRD) technique. The data were collected on a Bruker D8 Advance powder diffractometer employing Cu K_α radiation (U = 40 kV and I = 40 mA) and LynxEye detector. The measurements range was 10°–100° 2θ with step of 0.04° 2θ. The crystalline phases were identified by means of International Centre for Diffraction Data (ICDD) powder diffraction files. The unit cell parameters and mean size of the coherently scattering domains (LVol-IB) were obtained through the analysis of line positions and profile broadening by using the fundamental parameters peak shape description including appropriate corrections for the instrumental broadening and diffractometer geometry with the program TOPAS V4.2.

The texture characteristics were performed by low-temperature (− 196 °C) nitrogen adsorption using Quantachrome Instruments NOVA 1200e (USA) apparatus. Prior to the measurements, the samples were outgassed for 17 h at 110 °C under vacuum. The nitrogen adsorption–desorption isotherms were inspected to

estimate the specific surface area (S_{BET}), definite on the basis of the Brunauer, Emmett, Teller (BET) equation from the linear part of the isotherms. Total pore volume (V_t) and average pore diameter (d_{av}) were determined in accordance with the Gurvich rule at a relative pressure p/p_0 of 0.99. The pore size distribution (PSD) was specified from the desorption branch of the isotherms using Barrett–Joyner–Halenda (BJH) method.

X-ray photoelectron spectroscopy (XPS) measurements were accomplished on an AXIS Supra electron spectrometer (Kratos Analyical Ltd.) with base vacuum in the analysis chamber in the order of 10^{-8} Pa. The samples were irradiated with Mg K_α photons with energy of 1486.6 eV. The photo emitted electrons were separated, according to their kinetic energy, by an 180°-hemispherical analyzer with a total instrumental resolution of ~ 1.0 eV (as measured by the FWHM of Ag $3d_{5/2}$ line) at pass energy of 20 eV. Due to charging effect a resolution of ~ 1.3 eV has been measured on the isolated samples. Energy calibration was performed by normalizing the C 1s line of adventitious adsorbed hydrocarbons to 285.0 eV. The diameter of the analysis area was 750 μ. The concentrations (in at.%) of the observed chemical elements were calculated by normalizing the areas of their most intense photoelectron peaks to their relative sensitivity factors using the commercial software of the spectrometer.

WGS activity tests were carried out in a fixed-bed flow reactor at atmospheric pressure. For each measurement, 0.5 cm^3 catalyst bed volume with 0.63–0.80 mm grain size were loaded into a reactor. The WGS activity measurements were accomplished by means of reactant gaseous mixture of 3.76 vol% CO, 25.01 vol% H_2O and 71.23 vol% Ar in the temperature range 120–300 °C by step-wise increase of the reaction temperature and gas hour space velocity (GHSV) of 4000 h^{-1}. The WGS activity was expressed by the degree of CO conversion after achievement of a stationary CO conversion (at every 20 °C step) at the reactor outlet. The amount of residual CO was measured using URAS-3G gas analyzer (Hartmann&Braun AG). The degree of CO conversion was calculated on the basis of inlet and outlet CO concentrations. Additionally, analysis of the outlet gaseous mixture was performed by a HP5890 series II gas chromatograph equipped with a thermal conductivity detector and Carboxen-1000 column.

Results and discussion

Chemical analysis

The chemical composition of the NiAl samples listed in Table 1 discloses that Ni^{2+}/Al^{3+} molar ratio in the as-synthesized materials determinate by ICP is close to that in the mixed NiAl nitrate solution used for the sample preparation. The oxide form of the components is also shown for easily understanding. The estimated gold loading in Au-containing samples is also included in the Table 1.

Catalytic activity

The CO conversion over all the studied catalysts as a function of the temperature during WGSR is represented in Fig. 1.

It is noticeable, that the temperature induces the activity rising for the NiAl catalysts. A more significant difference in the WGS activity is observed in the interval 220–260 °C where the effect of Ni loading (Ni^{2+}/Al^{3+} molar ratio) is evident. Comparison of all catalysts activity discloses that NiAl2.5 catalyst shows 98.8% CO conversion at 260 °C, i.e. CO almost reaches the equilibrium conversion degree. The rest of catalysts demonstrate lower activity at the same reaction temperature, namely 92.6% CO conversion are achieved over NiAl4.0 and 36.1% over NiAl1.5. Based on these results, the deposition of Au was carried out on both active NiAl2.5 and NiAl4.0 catalysts. It is visible that the presence of Au markedly improves the conversion of CO therefore gold catalysts exhibit higher activity than their NiAl analogues. The promoting effect of Au is clearly presented by Au–NiAl2.5 catalyst which displays CO conversion of 97.6% at 240 °C. Unlike it, Au–NiAl4.0 catalyst shows approximately 11% lower activity at the same reaction temperature, i.e. 87.1% conversion of CO. Further increase of the reaction temperature to 260 °C leads to the 100% CO conversion over Au–NiAl2.5 catalyst and 98.6% over Au–NiAl4.0 one.

The reaction rate (r) at 180 °C was calculated for better representation of the differences in the WGS performance of the gold-containing catalysts. The obtained data indicate higher reaction rate ($mol_{COconv}\ g_{Au}^{-1}\ s^{-1} \times 10^{-5}$) for Au–NiAl2.5 catalyst (1.63) as opposed to Au–NiAl2.5 (1.49), thus confirming the higher WGS activity of Au-doped NiAl2.5 catalyst at lower reaction temperatures.

It should be underlined, that we use the concept of reaction rate for more detailed activity presentation of Au-containing catalysts instead of turnover frequency (TOF). The reason is that the TOF concept is the subject of debate in the catalytic community at present. As it has been reported in some articles and comments, the use of TOF is unjustified, the reaction rate can be used with a lot less contradiction instead [24–26].

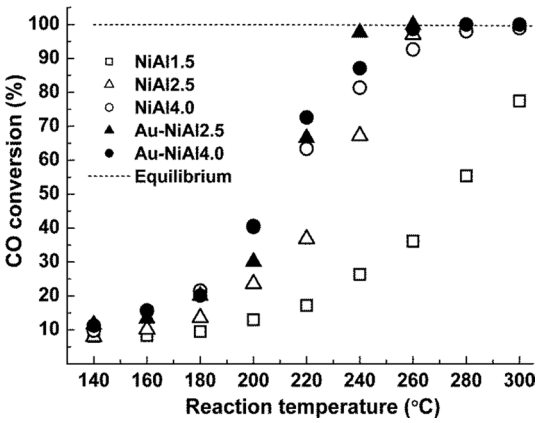

Fig. 1 The temperature dependence of CO conversion during WGSR over studied catalysts

It is well known that nickel catalysts are very active in the hydrogenation of CO and CO_2 to methane (methanation reaction). The advanced conversion of CO causes some doubt that this activity may include partial hydrogenation of CO by hydrogen to methane as a reaction product of WGSR. For this purpose, the outlet gaseous mixtures of the non-promoted and Au-promoted catalysts with the highest Ni concentration (NiAl4.0) were analyzed. The chromatographic analysis showed that the methane content was 0.46 wt% for NiAl4.0 and 0.48 wt% for Au–NiAl4.0. The results confirm that only the WGS reaction takes place over the studied catalysts in the investigated temperature range.

Powder X-ray diffraction

PXRD patterns of the as-synthesized NiAl samples (Fig. 2a) consist of reflections located at the angles typical of the stoichiometric takovite-type structure (ICDD-PDF file 00-015-0087). The patterns contain three sets of reflections namely sharp and symmetrical peaks which correspond to basal reflections (003) and (006), sharp

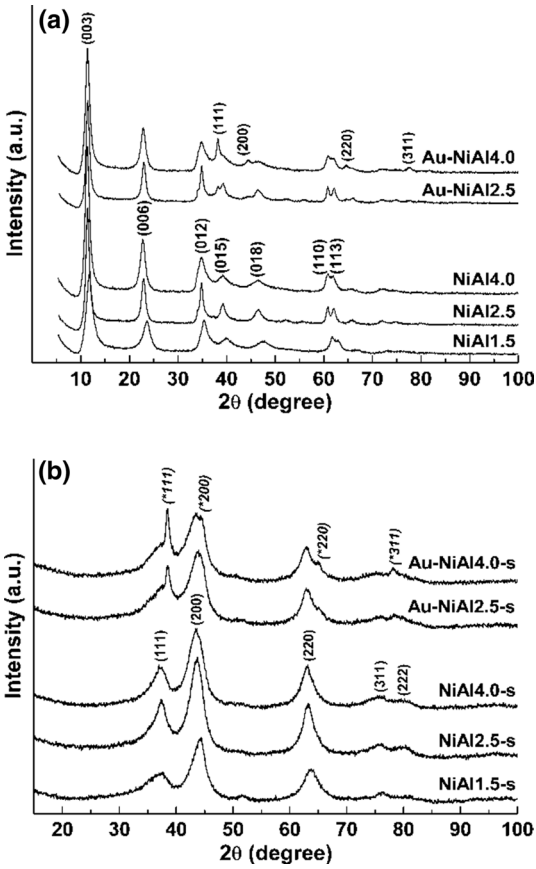

Fig. 2 PXRD patterns of the studied samples: as-prepared (**a**) and spent (**b**). The diffraction lines of gold phase are marked by asterisks and italic type

(110) and (113) reflections as well as broad and asymmetric (012), (015), and (018). It should be noted that the increase of Ni^{2+}/Al^{3+} molar ratio prompts slight shifting of all diffraction peaks towards lower values of 2θ angles, due to the lattice expansion [27]. The comparison indicates that NiAl samples display diffraction lines with different crystallinity. Since the well resolved doublet of the reflections (110) and (113) is associated with high degree of sample crystallinity [18] as well as with good ordering of the cations in the layers [28] it was found that NiAl2.5 sample is the best among the studied ones. In contrast, a gradual decrease of the peak intensities and broadening of the diffraction lines are observed when Ni^{2+}/Al^{3+} molar ratio differs from 2.5. This finding may be related to the existence of amorphous phases containing Ni^{2+}-entities in NiAl4.0 sample, or Al^{3+}-species in NiAl1.5, associated with the TKl structure [29]. Thus, PXRD study reveals the formation of a well-crystallized single TKl phase only in NiAl2.5 suggesting a high homogeneity of the sample.

The peaks in the diffraction patterns of as-prepared NiAl samples were indexed in a hexagonal cell with rhombohedral crystal symmetry of takovite containing carbonate ions in the interlayer space. The unit cell parameters and the crystallite size of the samples were calculated and presented in Table 2.

As it may be seen, the increase of Ni^{2+}/Al^{3+} molar ratio induces increase of the unit cell parameters a_{TK}, c_{TK} and V_{TK}, that is typical feature for the LDH materials [18]. The value of a_{TK} parameter corresponds to the distance between cations within the brucite-type layers and therefore it is very sensitive to the ionic radii of the cations [30]. The increase in the a_{TK} parameter is correlated with the higher octahedral ionic radius of Ni^{2+} (0.069 nm) with respect to Al^{3+} (0.050 nm) one [31], whereas the increase in c_{TK} parameter and volume -V_{TK} is related to the substitution of Al^{3+} by Ni^{2+} ions (Ni^{2+}/Al^{3+} molar ratio) and may be interpreted on the basis of electrostatic interaction. With increase of Ni^{2+}/Al^{3+} molar ratio, the extent of interaction between the hydroxide layer and interlayer diminishes with effective increase in the interlayer gallery [30]. The decrease of parameter a_{TK} for NiAl4.0 suggests co-existence of NiAl LDH phase and another one rich in Ni^{2+} ions, and very likely XRD amorphous. The presence of last phase is responsible for the partially amorphization of the TKl structure. The different sample crystallinity is evidenced by estimating the mean crystallite sizes (L_{TK}) of the TKl phase. The better crystallized NiAl2.5 solid possesses crystallites of larger size while the poorly crystallized NiAl1.5 shows smaller size.

As it was mentioned above, to understand the influence of gold on the activity in WGSR, the more active NiAl catalysts (NiAl2.5 and NiAl4.0) were used as carriers for obtaining of gold catalysts. Notably, the deposition of Au on both samples prompts appearance of additional reflections at 2θ = 38.2°, 44.4°, 64.6° and 77.5° which are attributable to (111), (200), (220) and (311) lines, characteristic of face centered-cubic metal Au phase (ICDD-PDF file 00-004-0784), better formed in Au–NiAl4.0 (Fig. 2b). In the figure, the diffraction lines of gold phase are marked by asterisks and italic type. The PXRD of Au-containing samples confirm that gold particles are deposited on NiAl LDHs successfully. Both samples exhibit the characteristic diffraction lines of layered TKl material, indicating that addition of Au does not destroy the layered structure. The similarity of the lattice parameters and the mean crystallite sizes values of TKl phase in the samples with and without gold

Table 2 Structural characteristics of the studied samples

Sample	a_{TK} (nm)	c_{TK} (nm)	V_{TK} (nm^3)	L_{TK} (nm)	a_{NiO} (nm)	V_{NiO} (nm^3)	L_{NiO} (nm)	a_{Au} (nm)	V_{Au} (nm^3)	L_{Au} (nm)
NiAl1.5	0.3007 (8)	2.257 (7)	0.1770 (2)	5.6	–	–	–	–	–	–
NiAl2.5	0.3044 (1)	2.323 (1)	0.1868 (1)	11.0	–	–	–	–	–	–
NiAl4.0	0.3029 (1)	2.326 (2)	0.1848 (1)	8.8	–	–	–	–	–	–
Au–NiAl2.5	0.3043 (1)	2.319 (2)	0.1859 (2)	11.0	–	–	–	0.4075 (2)	0.0676 (1)	15.0
Au–NiAl4.0	0.3031 (2)	2.325 (2)	0.1848 (1)	8.5	–	–	–	0.4070 (2)	0.0674 (2)	14.6
NiAl1.5-s	–	–	–	–	0.4127 (7)	0.0702 (2)	3.3	–	–	–
NiAl2.5-s	–	–	–	–	0.4158 (4)	0.0718 (1)	3.7	–	–	–
NiAl4.0-s	–	–	–	–	0.4167 (6)	0.0722 (2)	3.4	–	–	–
Au–NiAl2.5-s	–	–	–	–	0.4184 (5)	0.0731 (2)	3.0	0.4073 (4)	0.0675 (2)	19.6
Au–NiAl4.0-s	–	–	–	–	0.4182 (4)	0.0726 (2)	2.7	0.4064 (3)	0.0665 (1)	20.3
Takovite[a]	0.3025	2.259	0.1791	–	–	–	–	–	–	–
Gold[b]	–	–	–	–	–	–	–	0.4078	0.0678	–
NiO[c]	–	–	–	–	0.4177	0.0729	–	–	–	–

[a]ICDD 00-015-0087

[b]ICDD 00-004-0784

[c]ICDD 00-004-0835

confirms this statement. The metal Au lattice parameters and mean crystallite sizes show very close values in both Au-containing samples (Table 2).

PXRD analyses of all tested in WGSR catalysts (Fig. 2b) display reflections indexed as (111), (200), (220), (311) and (222) of cubic NiO phase (JCPDS file 00-047-1049), which are better pronounced in NiAl2.5-s. Inspection of the PXRD patterns indicates poorly crystalline state presumably related to the formation of very small crystals for the main NiO phase. The data presented in Table 2 reveals nano-scaled NiO phase with mean crystallite size 3–4 nm for NiAl catalysts and smaller for Au-doped NiAl ones (3.0 nm). The data specify a higher dispersion of the active NiO phase in the presence of gold nanoparticles. In addition, the observed broadening of NiO diffraction lines is due to Al^{3+} ions incorporation into the cubic framework of NiO reducing its cell parameter dimensions, a_{NiO} and V_{NiO}, versus standard NiO because of the smaller radius of Al^{3+} species as compared to Ni^{2+} ones [32]. The increase of a_{NiO} and V_{NiO} parameters of Au-containing spent catalysts, especially in Au-NiAl2.5-s may be due to the effect of Au to provoke an increase of Ni^{3+} ions thus leading to an increased number of cationic vacancies (which have a larger radius) and consequently to a larger parameters or any mutual influences of the lattices of the two phases associated with strains of the grains boundary (effect of the composite).

It can be noted that the alterations in the degree of sample crystallinity in as-prepared layered systems are preserved with respect to the NiO structure in the tested catalysts, being better organized in NiAl2.5-s. Furthermore, the nano-scaled magnitudes of TKl phase in the as-synthesized samples (Table 2) generate also nano-metrical NiAl mixed oxides of the type $Ni^{2+}(Al^{3+})O$ [18]. The sharp diffraction peaks especially at $2\theta = 38.2°$ reveal high crystallinity of the gold phase which is consistent with the crystallite size values. The tendency to better formation of gold phase in NiAl4.0 material is retain in the case of spent Au–NiAl4.0-s catalyst.

No metallic nickel (that facilitates methanation reaction) was registered in the temperature range investigated, thus sustaining the statement from chromatographic analysis of the outlet gaseous mixtures that only WGS reaction takes place over the studied catalysts.

N_2-physisorption analysis

The change of texture parameters and pore size distribution (PSD) of NiAl2.5 sample after deposition of gold (Au–NiAl2.5) was investigated by N_2-physisorption study before and after WGS reaction.

The N_2 adsorption–desorption isotherms of NiAl2.5 and Au–NiAl2.5 samples are presented in Fig. 3a. The isotherm types and hysteresis loops were determined in accordance with Rouquerol et al. [33] and Thommes et al. [34]. The isotherm of NiAl2.5 sample may be classified as type II specific for nonporous or macroporous solids. The observed hysteresis loop H3 type is usually found in materials consisting of aggregates of plate-like particles having non-rigid slit-shaped pores and specifies the presence of mesopores and is consistent with the mesoporous nature of the LDH samples [18]. The character of the isotherm type is preserved after

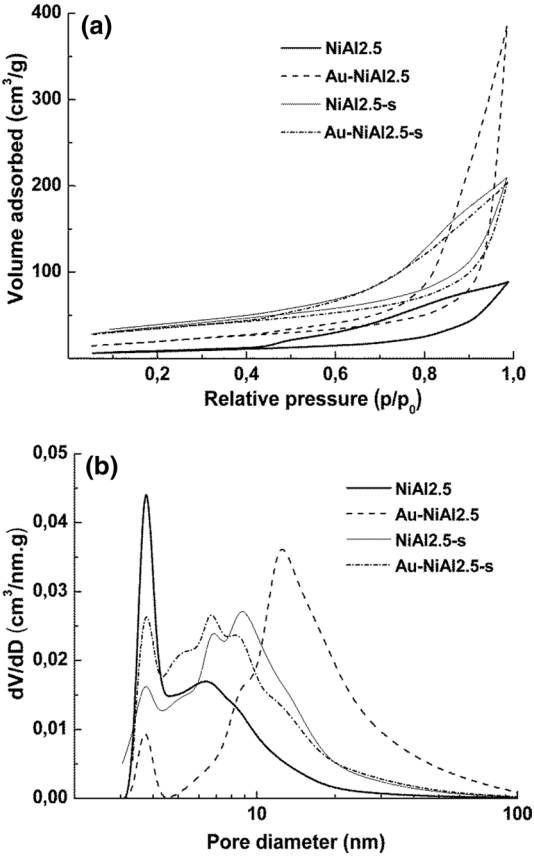

Fig. 3 The texture characteristics of NiAl2.5 and Au–NiAl2.5 samples: nitrogen adsorption–desorption isotherms (**a**) and pore size distribution (**b**)

deposition–precipitation of gold over NiAl2.5 sample (Fig. 3a). The rising of H3 hysteresis loop at higher p/p_0 indicates generation of new mesopores which explains the twofold increase of the texture parameters as S_{BET}, V_t and d_{av} of Au–NiAl2.5 sample (Table 3).

PSD profiles calculated by BJH method of the as-synthesized samples illustrate that Au-free sample exhibits bimodal type of distribution (Fig. 3b) in the range of 1–30 nm with two maxima: intensive at 3.8 nm and wider at 6.5 nm. A change of PSD picture is observed after gold deposition on NiAl2.5 solid. The larger particles of Au phase with 15 nm in size (Table 2) is a reason for the blocking of smaller

Table 3 Texture parameters of NiAl2.5 and Au–NiAl2.5 samples

Sample	S_{BET} (m^2/g)	V_t (cm^3/g)	d_{av} (nm)
NiAl2.5	30	0.14	18.3
Au–NiAl2.5	74	0.60	32.4
NiAl2.5-s	129	0.33	10.1
Au–NiAl2.5-s	123	0.32	10.3

mesopores of NiAl2.5 sample with diameter between 2.0 and 8.0 nm. The new mesopores with larger diameters in the range 8–100 nm are registered as a result of Au particle deposition on the TKl surface. This observation is a precondition for creation of greater number sites for adsorption of CO molecules on the surface of Au–NiAl2.5 sample, which could be responsible for higher catalytic activity in the WGSR.

N_2 physisorption study of both spent catalysts establishes identical isotherms with preserved type (Fig. 3a) due to phase transformation of the layered structure to NiO phase under the impact of the reaction medium, as was disclosed by PXRD study. The structural changes lead to close values of texture parameters for both tested catalysts. One additional reason for increase of S_{BET} is formation of micropores which can be seen by the registered intercept on the ordinate (Fig. 3a), which indicates the presence of micropores. PSD profiles of both spent catalysts have a similar shape characterizing poly-dispersed type of distribution (Fig. 3b).

XPS experiments

A possible understanding and explanation of the observed activity in WGSR and information about the surface oxidation state of catalytically active species may be found in the results obtained from the characterization of the most active Au–NiAl2.5 catalyst by XPS. Particular attention was paid to the oxidation state of nickel, which is a major component in the catalytic systems, thus Ni2*p* spectra (Fig. 4a) and O 1s core level (Fig. 4b) of Au–NiAl2.5 were carefully analyzed.

The existence of Ni^{2+} ions in as-synthesized Au–NiAl2.5 sample is recognized by the Ni2*p* spectrum, namely Ni2$p_{3/2}$ peak at 855.9 eV and Ni2$p_{1/2}$ peak at 873.7 eV as well as with two satellites at 861.6 and 879.7 eV (Fig. 4a). The binding energy (BE) value of the main Ni2$p_{3/2}$ peak at 855.9 eV (Table 4) can be attributed to Ni^{2+} ions in $Ni(OH)_2$ from brucite-like layers of TKl structure in accordance with the BE value for Ni2$p_{3/2}$ photoelectrons in $Ni(OH)_2$ (855.6–856.6 eV) [35]. The O 1s core level (Fig. 4b) represents a symmetrical peak at 531.3 eV which testifies to oxygen from the OH group in $Ni(OH)_2$ [36, 37].

The spectrum of spent Au–NiAl2.5 catalyst in the Ni2$p_{3/2}$ region shows peak at 855.9 eV that is wider in comparison with that of the as-synthesized sample and it approves Ni^{2+} ions with oxygen surrounding (Fig. 4a).

The deconvolution of Ni2p level reveals existence of second peak at 857.7 eV that is ascribed to Ni^{3+} ions in surface oxygen species as Ni–OOH [35]. The presence of more Ni–O structures is confirmed from the shape of O 1*s* core level, which is broader and asymmetrical towards higher BE (Fig. 4b). The curve fitting of the peak displays two basic states of oxygen at 531.4 eV corresponding to oxygen from the OH group in $Ni(OH)_2$ and another peak at 534.3 eV that can be interpreted as surface oxygen intermediates such as Ni–OOH containing Ni^{3+} ions [38]. The O surface concentrations (Table 4) support this finding.

The XPS measurements and data collected in Table 4 indicated that nickel presents as Ni^{2+} oxidation state in the same concentrations on the surface of fresh Au–NiAl2.5 and spent Au-NiAl2.5-s catalysts, values describing Ni^{2+} state in

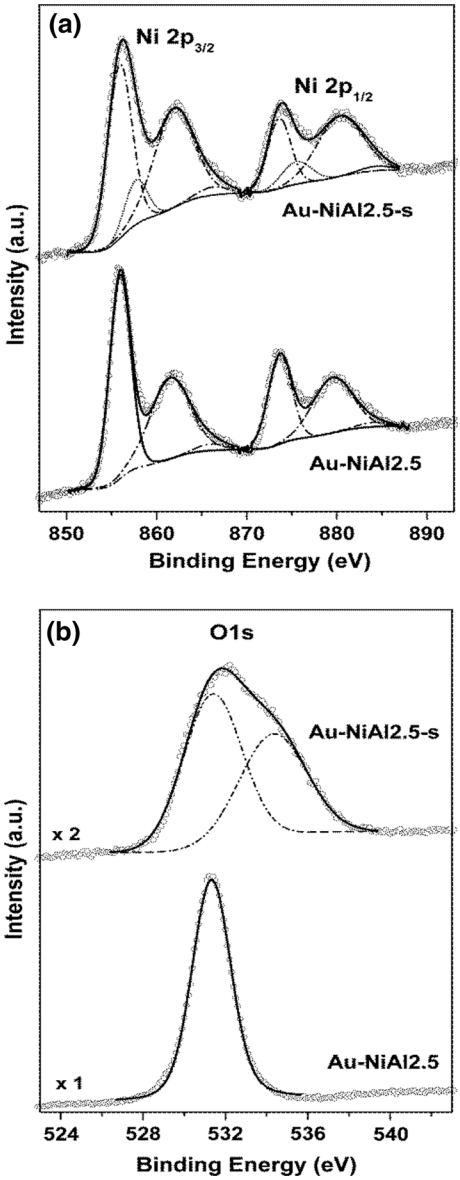

Fig. 4 XPS spectra of Au–NiAl2.5 and Au–NiAl2.5-s samples: Ni2*p* spectra (**a**) and O 1*s* core level (**b**)

Table 4 XPS data of the as-synthesized Au–NiAl2.5 and spent Au–NiAl2.5-s samples

Sample	Binding energy (eV)						Surface concentrations (at.%)					
	Ni2$p_{3/2}$		Au4$f_{7/2}$	Al2*p*	O 1*s*		Ni^{2+}	Ni^{3+}	Au	Al	O1	O2
Au–NiAl2.5	855.9	–	84.0	73.8	531.3	–	23.3	–	0.1	8.3	68.3	–
Au–NiAl2.5-s	855.9	857.7	84.0	74.4	531.4	534.3	23.7	5.4	0.1	12.4	33.2	25.2

Ni–O species. In addition, Ni^{3+} oxidation state on the surface of the spent catalyst discloses presence of Ni^{3+}OOH hydroxide structures. The Al2p core level show peaks at about 74 eV that is ascribed to Al^{3+} species (Al–O) [27] signifying higher concentration of Al–O structures on the surface of the spent catalyst. The existence of metallic gold on the surface of fresh Au–NiAl2.5 and spent Au–NiAl2.5-s catalysts is proved by BE at about 84 eV for Au4$f_{7/2}$ level [39]. Moreover, the concentration of metallic gold on the surface of spent Au–NiAl2.5-s catalyst is preserved after the WGSR.

PXRD and XPS analyses were used to get more insight into the correlation between the catalytic activity and the electronic structure of Au–NiAl catalysts. The layered structure collapses accompanied by the appearance of NiO phase during the time on stream at elevated temperature, as it was disclosed above. The large amount of water vapor in the reaction mixture is expected to cause partial hydroxylation of the NiO surface with formation of $Ni(OH)_2$ and NiOOH structures, containing Ni^{2+} and Ni^{3+} cations. It was supposed in our previous paper [5] that the redox WGSR proceeds over Ni-containing catalytic entities via an associative reaction mechanism. It considers the interaction between adsorbed CO molecule and surface OH groups resulting in formation of specific surface complex containing active OH groups, intermediate formate species (carbonate or bicarbonate are also possible), and reversible redox $Ni^{2+} \leftrightarrow Ni^{3+}$ transition. Finally, the complex decomposes to the reaction products, CO_2 and H_2. Redox transfer and capability of the nickel hydroxide structures to intercalate H_2O molecules support the associative mechanism.

The presence of Ni^{2+} and Ni^{3+} ions in the hydroxides specifies their role as active structures in the WGSR reaction. The participation of the nickel-hydroxide phases in the redox WGS reaction can be related to the reversible redox process between nickel ions ($Ni^{2+} \leftrightarrow Ni^{3+}$) analogous to the processes performed on the positive electrodes of nickel alkaline storage batteries: $Ni(OH)_2 + xOH^- \leftrightarrow NiO_2 H_{2-x} + xH_2O + xe^-$ [40]. It should be pointed out that, the availability of nickel in both Ni^{2+} and Ni^{3+} oxidation states on the catalyst surface contributes to the demonstrated high activity in the studied temperature range.

The role of gold addition to NiAl samples was to favor creation of the working composition on the catalyst surface and to contribute to CO activation. By analyzing the activity of gold-based catalysts, it is often important to stress on the role of gold particles size. The availability of small gold particles (below 5 nm) as well as highly dispersed gold clusters was shown beneficial for high WGS activity [41]. In the present study were observed relatively larger gold nanoparticles (15–20 nm) and future efforts could be focused on tuning the experimental conditions in order to deposit gold in highly dispersed state. However, the formation of larger gold particles on the surface of NiAl LDH has an advantage. Boccuzzi et al. [42] have found spectroscopic evidences for hydrogen dissociation on small metallic gold particles even at room temperature, producing active hydrogen atoms that can spillover on the support and caused reduction of the support surface sites. Such phenomenon is undesired, because metallic nickel governs methanation—a side reaction that consumes hydrogen and should be avoided during WGSR.

Stability test

Considering catalytic behavior of Au-based catalysts and possibility for their practical application, it is always important to analyze catalyst stability. One reason very often discussed for decreased activity is agglomeration of gold nanoparticles during the catalytic tests. Although our PXRD results indicated a slight increase of the gold particle size after WGRS, the stability test performed with the most active Au–NiAl2.5 catalyst demonstrated the same CO conversion degree within 32 h on stream at 260 °C.

Conclusions

It can be deduced from the results obtained in this study that the NiAl LDHs with Ni^{2+}/Al^{3+} molar ratio of 2.5 and 4.0 can be applied as catalysts as well as supports for gold catalysts in WGSR.

The WGS activity is strongly affected by the nickel loading (Ni^{2+}/Al^{3+} molar ratio) and the presence of gold, and is related to the existence of surface Ni^{2+} and Ni^{3+} ions, which are responsible for the reversible redox $Ni^{2+} \leftrightarrow Ni^{3+}$ transition.

Probable scheme is proposed about reaction mechanism, comprising redox $Ni^{2+} \leftrightarrow Ni^{3+}$ transition on the catalyst surface as well as adsorption and activation of CO molecule on Au particles.

The effect of supported gold is more significant in the catalyst with lower Ni amount (Au–NiAl2.5), thus permits obtaining and using of promising and cost-effective catalyst for medium-temperature WGSR. The catalyst is active enough to carry out the process in only one step at medium temperatures, decreasing the operational costs.

Acknowledgements The authors T.T. and I.I. gratefully acknowledge financial support by the Bulgarian National Science Fund (Contract ДН 09/5/2016). This work was partially supported by the Bulgarian Ministry of Education and Science under the National Research Programme E+: Low Carbon Energy for the Transport and Households, grant agreement D01-214/2018.

References

1. Tao F, Ma Z (2013) Water-gas shift on gold catalysts: catalyst systems and fundamental studies. Phys Chem Chem Phys 15:15260–15270
2. Pal DB, Chand R, Upadhyay SN, Mishra PK (2018) Performance of water gas shift reaction catalysts: a review. Renew Sust Energy Rev 93:549–565
3. Reddy GK, Smirniotis PG (2015) Water gas shift reaction: research developments and applications. Elsevier, Amsterdam
4. Fuentes E, Jùnior A, Silva T, Assaf J, Rangel M (2011) A comparison between copper and nickel-based catalysts obtained from hydrotalcite-like precursors for WGSR. Catal Today 171:290–296
5. Andreev A, Idakiev V, Kostov K, Gabrovska M (1995) Water-gas shift reaction over nickel hydroxides. Catal Lett 31(2–3):245–252

6. Gabrovska M, Edreva-Kardjieva R, Idakiev V, Kunev B (2002) Influence of Mg on the Structure and the properties of Ni-Al takovite-like material. Bulg Chem Commun 34(3/4):395–404
7. Gabrovska M, Idakiev V, Tenchev K, Nikolova D, Edreva-Kardjieva R, Crisan D (2013) Catalytic performance of Ni-Al layered double hydroxides in CO purification processes. Russ J Phys Chem A 87(13):2152–2159
8. Reina TR, González MC, Palma S, Ivanova S, Odriozola JA (2014) Twenty years of golden future in the water gas shift reaction. In: Ma Z, Dai S (eds) Heterogeneous gold catalysts and catalysis, vol 18. RSC Catal Series, Royal Society of Chemistry, Cambridge, pp 111–140
9. Qi C, Amphlett JC, Peppley BA (2005) Methanol steam reforming over NiAl and Ni(M)Al layered double hydroxides (M = Au, Rh, Ir) derived catalysts. Cat Lett 104(1–2):57–62
10. Andreeva D, Idakiev V, Tabakova T, Andreev A (1996) Low-temperature water-gas shift reaction over Au/α-Fe_2O_3. J Catal 158:275–283
11. Wang X, Rodriguez JA, Hanson JC, Perez M, Evans J (2005) In situ time-resolved characterization of Au-CeO_2 and AuOx-CeO_2 catalysts during the water-gas shift reaction: presence of Au and O vacancies in the active phase. J Chem Phys 123:221101
12. Sandoval A, Gomez-Cortes A, Zanella R, Diaz G, Saniger JM (2007) Gold nanoparticles: support effects for the WGS reaction. J Mol Catal A 278:200–208
13. Odabasi C, Günay ME, Yildirim R (2014) Knowledge extraction for water gas shift reaction over noble metal catalysts from publications in the literature between 2002 and 2012. Int J Hydr Energy 39:5733–5746
14. Andreeva D, Tabakova T, Ilieva L (2013) Ceria-based gold catalysts: synthesis, properties and catalytic performance for the WGS and PROX processes. In: Trovarelli A, Fornasiero P (eds) Catalysis by ceria and related materials, 2nd edn. Imperial College Press, London, p 497
15. Flytzani-Stephanopoulos M (2014) Gold atoms stabilized on various supports catalyze the water-gas shift reaction. ACC Chem Res 47(3):783–792
16. Yang M, Flytzani-Stephanopoulos M (2017) Design of single-atom metal catalysts on various supports for the low temperature water-gas shift reaction. Catal Today 298:216–225
17. Bish D, Brindley G (1977) A reinvestigation of takovite, a nickel-aluminium hydroxycarbonate of the pyroaurite group. Am Miner 62(5–6):458–464
18. Cavani F, Trifirò F, Vaccari A (1991) Hydrotalcite-type anionic clays: preparation, properties and applications. Catal Today 11:173–301
19. Thevenot F, Szymanski R, Chaumette P (1989) Al-rich Zn-Al hydrotalcite-like compounds. Clays Clay Miner 37:396–402
20. Vaccari A (1998) Preparation and catalytic properties of cationic and anionic clays. Catal Today 41:53–71
21. Vaccari A (1999) Clays and catalysis: a promising future. Appl Clay Sci 14:161–198
22. Zümreoglu-Karan B, Ay A (2012) Layered double hydroxides—multifunctional nanomaterials. Chem Pap 66(1):1–10
23. Andreeva D, Idakiev V, Tabakova T, Ilieva L, Falaras P, Bourlinos A, Travlos A (2002) A low-temperature water-gas shift reaction over Au/CeO_2 catalysts. Catal Today 72:51–57
24. Kozuch S, Martin JML (2012) "Turning Over" definitions in catalytic cycles. ACS Catal 2:2787–2794
25. Lente G (2013) Comment on "Turning Over" definitions in catalytic cycles. ACS Catal 3(3):381–382
26. Bligaard T, Morris RB, Campbell CT, Chen JG, Gates BC, Gorte RJ, Jones CW, Jones WD, Kitchin JR, Scott SL (2016) Toward benchmarking in catalysis science: best practices, challenges, and opportunities. ACS Catal 6:2590–2602
27. Guo D, Wang Y, Zhao P, Bai M, Xin H, Guo Z, Li J (2016) Selective aerobic oxidation of benzyl alcohol driven by visible light on gold nanoparticles supported on hydrotalcite modified by nickel ion. Catalysts 6(5):64
28. Benito P, Labajos F, Rives V (2006) Microwave-treated layered double hydroxides containing Ni^{2+} and Al^{3+}: the effect of added Zn^{2+}. J Solid State Chem 179:3784–3797
29. Gabrovska M, Edreva-Kardjieva R, Crişan D, Tzvetkov P, Shopska M, Shtereva I (2012) Ni-Al layered double hydroxides as catalyst precursors for CO_2 removal by methanation. React Kinet Mech Cat 105(1):79–99
30. Kannan S, Narayanan A, Swamy CS (1996) Effect of composition on the physicochemical properties of nickel aluminium hydrotalcites. J Mater Sci 31:2353–2360

31. Shannon R (1976) Revised effective ionic radii and systematic studies of interatomic distances in halides and chaleogenides. Acta Crystallogr A 32:751–767
32. Puxley DC, Kitchener IJ, Komodromos C, Parkyns ND (1983) The effect of preparation method upon the structures stability and metal/support interactions in nickel/alumina catalysts. Stud Surf Sci Catal 16:237–271
33. Rouquerol F, Rouquerol J, Sing K (1999) Adsorption by powders and porous solids, principle, methodology and applications. Academic Press, Cambridge
34. Thommes M, Kaneko K, Niemark AV, Olivier JP, Rodriguez-Reinoso F, Rouquerol J, Sing KSW (2015) Physisorption of gases, with special reference to the evaluation of surface area and pore size distribution (IUPAC Technical Report). Pure Appl Chem 87:1051–1069
35. Grosvenor AP, Biesinger MC, Smart RS, McIntyre NS (2006) New interpretations of XPS spectra of nickel metal and oxides. Surf Sci 600:1771–1779
36. Kim K, Winograd N (1974) X-ray photoelecton spectroscopic studies of nickel-oxygen surfaces using oxygen and argon ion-bombardment. Surf Sci 43:625–643
37. Barr TL (1978) An ESCA study of the termination of the passivation of elemental metals. J Phys Chem 82(16):1801–1810
38. Jindra J, Krejci I, Mrha J, Foekesson B, Johansson LY, Larsson R (1984) ESCA investigations on plastic-bonded nickel oxide electrodes. J Power Sources 13(2):123–136
39. Fang WH, Chen JS, Zhang QH, Deng WP, Wang Y (2011) Hydrotalcite-supported gold catalyst for the oxidant-free dehydrogenation of benzyl alcohol: studies on support and gold size effects. Chem Eur J 17:1247–1256
40. Oliva P, Leonardi J, Laurent J, Delmas C, Braconnier J, Figlarz M, Fievet F, de Guibert A (1982) Review of the structure and the electrochemistry of nickel hydroxides and oxy-hydroxides. J Power Sources 8:229–255
41. Tabakova T, Manzoli M, Vindigni F, Idakiev V, Boccuzzi F (2010) CO-free hydrogen production for fuel cell applications over Au/CeO_2 Catalysts: FTIR insight into the role of dopant. J Phys Chem A 114:3909–3915
42. Boccuzzi F, Chiorino A, Manzoli M, Andreeva D, Tabakova T (1998) FTIR study of the low-temperature water-gas shift reaction on Au/Fe_2O_3 and Au/TiO_2 catalysts. J Catal 188:176–185